# Reliable binary cell-fate decisions based on oscillations

B. Pfeuty[*]

*Laboratoire de Physique des Lasers, Atomes, et Molécules, CNRS, UMR 8523, Université Lille 1, F-59655 Villeneuve d'Ascq, France*

K. Kaneko

*Graduate School of Arts and Sciences, The University of Tokyo, Komaba, Meguro-ku, Tokyo 153-8902, Japan*

Biological systems have often to perform binary decisions under highly dynamic and noisy environments, such as during cell-fate determination. These decisions can be implemented by two main bifurcation mechanisms based on the transitions from either monostability or oscillation to bistability. We compare these two mechanisms by using stochastic models with time-varying fields and by establishing asymptotic formulas for the choice probabilities. Different scaling laws for decision sensitivity with respect to noise strength and signal timescale are obtained, supporting a role for oscillatory dynamics in performing noise-robust and temporally tunable binary decision-making. This result provides a rationale for recent experimental evidences showing that oscillatory expression of proteins often precedes binary cell-fate decisions.

## I. INTRODUCTION

Living organisms must constantly make important decisions in fluctuating environments. The characterization of the nonlinear behavior of interacting proteins and cells is key to understand how these organisms achieve appropriate decisions, such as during cellular differentiation. The differentiation process that generates a diversity of cell types in multicellular organisms occurs sequentially at various developmental stages, in which multipotent cells select between a finite number, typically two, lineage-specific cell types [1]. The outcomes of these successive two-choice decisions rely on the activity of specific intracellular regulatory networks under the influence of highly dynamic extracellular signals and various sources of stochasticity [2]. On the one hand, the role of noise is very ambivalent as it may contribute to beneficial phenotypic heterogeneity but may also lead to errors in signal-driven decisions [3]. On the other hand, the temporal properties of the signal are likely to subtly influence decision outcomes [4,5]. A fundamental issue is thus to understand how binary decisions are orchestrated by the interplay of signal and noise, in a manner that presumably depends on the local dynamics near a bifurcation point where the number of stable states changes [6].

From a dynamical-system viewpoint, binary cell-fate decision can be implemented by two main dynamical mechanisms [7]. The most prevalent mechanism relies on pitchfork bifurcation in which the trigger signal destabilizes the uncommitted steady state and switches toward two possible differentiation steady states [8–10]. This scenario is prone to arise in genetic circuits based on mutual activation or inhibition between self-activating regulators. However, an alternative mechanism, based on oscillatory dynamics, has also been proposed [11–13]. In this scenario, binary choice coincides with the transition from oscillations to bistability, which is likely to occur in biochemical networks combining positive and negative feedback loops [14]. These transition and feedback

properties are found in many signaling and regulatory molecular pathways that drive binary cell-fate decisions [15–17].

## II. BINARY DECISION MODEL

In contrast with previous cell differentiation models relying on numerical simulations and bifurcation analysis of protein and cellular networks [8–13], we use here an analytical approach in order to compare the two decision-making scenarios above, with respect to the controversial effects of noise and signal timing. To this aim, the dynamics of one decision unit (e.g., the cell) is simply described by the following Langevin equation:

$$\frac{dx}{dt} = F(x, \alpha, s(t, \tau)) + \sigma \zeta(t), \quad (1)$$

where the decision trigger signal $s$ can be modeled to first approximation by a saturating exponential with time scale $\tau$:

$$s(t, \tau) = \begin{cases} 0, & t \leqslant 0 \\ 1 - e^{-t/\tau}, & t \geqslant 0. \end{cases} \quad (2)$$

First, we consider one-dimensional dynamical systems whose scalar field derives from a potential as $F(x, \alpha, s(t)) = -\frac{\partial U(x, \alpha, s(t))}{\partial x}$. To implement a binary decision, the force field $F(x, 0, s)$ is assumed to exhibit two stable fixed points $x_A$ and $x_B$ (i.e., cell-fate attractors $\mathcal{A}$ and $\mathcal{B}$) for $s$ above some threshold ($s_c = 0.5$), whereas the parameter $\alpha$ biases the stability of one attractor relative to the other. The effect of noise is taken into account by a stochastic term where $\zeta(t)$ is zero-mean Gaussian white noise with unit variance and $\sigma$ is the noise strength. In this model, the interplay among signal increase (with the rise time $\tau$), noise (of intensity $\sigma$), and the bias parameter ($\alpha$) determines the respective probabilities $\mathcal{P}_A$ and $\mathcal{P}_B$ to select, after some time, attractors $\mathcal{A}$ or $\mathcal{B}$ [Fig. 1(a)]. For simplicity, but not necessity, we consider that the force field is endowed with symmetries that ensure equiprobable attractor selection $\mathcal{P}_A = \mathcal{P}_B$ for $\alpha = 0$ and that $\mathcal{P}_A(\alpha) = \mathcal{P}_B(-\alpha)$ otherwise. By convention, we define $\mathcal{A}$ (respective to $\mathcal{B}$) as $\mathcal{P}_A > 0$ for $\alpha > 0$. In this model, essential features of decision making can be
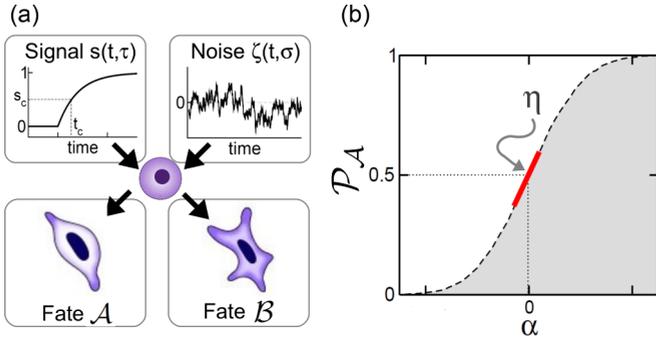
FIG. 1. (Color online) (a) Binary cell-fate decision driven by the interplay of signal and noise. (b) Binary choice sensitivity measure $\eta$.

captured by the following decision sensitivity quantity:

$$\eta = \frac{d\mathcal{P}_{\mathcal{A}}}{d\alpha}\bigg|_{\alpha=0}, \tag{3}$$

which measures the infinitesimal choice probability changes induced by the selection bias parameter $\alpha$ [Fig. 1(b)]. The significance of $\eta$ values is assessed in the context of probabilistic theory of biological (including cognitive) decision making under uncertainty [18,19], which presupposes a statistical rather than deterministic relationship between the selection bias parameter (i.e., $\alpha$) and the appropriateness or fitness of the decision. According to this theory, optimal decision in an uncertain environment is associated with a smooth function $\mathcal{P}_{\mathcal{A}/\mathcal{B}}(\alpha)$ of some intermediate $\eta$ value. Because the noise strength $\sigma$ is likely to represent the combined effect of multiple sources of intratrial and intertrial variabilities and $\tau$ is one important timescale of the decision process, the manner how $\eta$ depends on these two parameters provides valuable insights into trial-to-trial reliability and temporal control of binary decision making. We restrict our study to $\sigma$ not too large, thereby disregarding the case where attractor selection is influenced by noise-induced transition between $\mathcal{A}$ and $\mathcal{B}$ when decision trigger signal is switched on. Such an assumption is motivated by the biological context of multicellular development where spontaneous transdifferentiation events are unlikely.

Given these general binary-decision model and quantities, the goal is now to compare the decision properties associated with two time-varying force fields $F(x,\alpha,s(t))$ [and potentials $U(x,\alpha,s(t))$] that implements in a minimal manner the two bifurcation scenarios based on the transitions from either monostability or oscillation to bistability.

## III. PITCHFORK MECHANISM

### A. Transition from monostability to bistability

The prevalent model for binary decisions involves a pitchfork bifurcation scenario, such as for cell differentiation where the interplay between multiple positive feedback loops in protein regulatory networks typically implement a subcritical pitchfork bifurcation mechanism [8–10]. The simplest scalar field associated with this bifurcation scenario is given by

$$F_P(x,\alpha,s) = \alpha + \beta_1(s - 0.5)x + \beta_2 x^3 - x^5, \tag{4}$$



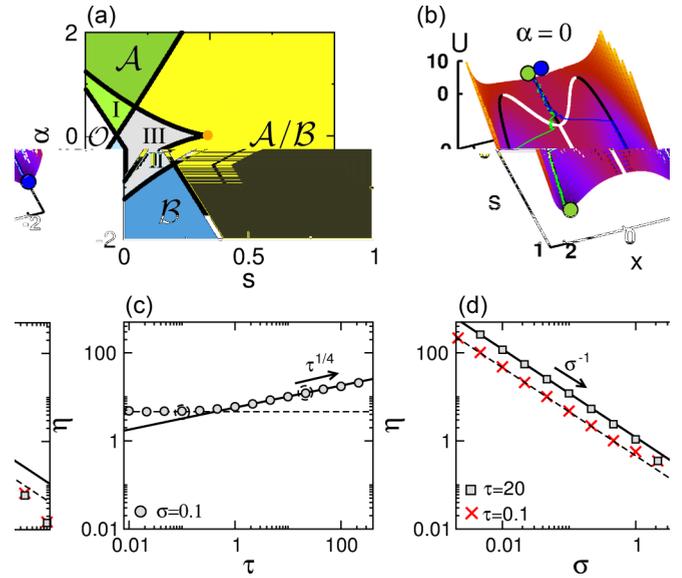FIG. 2. (Color online) Binary decision making based on pitchfork bifurcation [Eq. (4) with $\beta_1 = 6$ and $\beta_2 = 3$]. (a) Phase diagram where $s$ is considered as a parameter and $\mathcal{O}$, $\mathcal{A}$, and $\mathcal{B}$ are steady states. Multistable domains I, II, and III correspond to $\mathcal{O}/\mathcal{A}$, $\mathcal{O}/\mathcal{B}$, and $\mathcal{O}/\mathcal{A}/\mathcal{B}$, respectively. (b) Potential landscape and bifurcation diagram [black (white) lines: stable (unstable) steady-state branches] for $\alpha = 0$ with two examples of noisy trajectories. (c), (d) $\eta$ as a function of $\tau$ and $\sigma$ in numerical simulations (circles, squares, and crosses) as compared with the theoretical predictions of Eqs. (10) (solid lines) and (11) (dashed lines).

where $\beta_1 > 0$. In the symmetric case ($\alpha = 0$), a pitchfork bifurcation occurs for $s \equiv s_c = 0.5$ at time $t \equiv t_c = \tau \ln 2$. A positive value for $\beta_2$ ensures that the bifurcation is subcritical. The symmetry-breaking term $\alpha$ results instead in an imperfect pitchfork bifurcation. As a function of $\alpha$ and $s$ (considered first as a parameter), the phase diagram displays three stable steady states $\mathcal{O}$, $\mathcal{A}$, and $\mathcal{B}$ with specific domains of multistability ($\mathcal{O}/A$, $\mathcal{O}/B$, $\mathcal{O}/A/B$, and $\mathcal{A}/\mathcal{B}$) [Fig. 2(a)]. In the small $\sigma$ and $\alpha$ limit, temporal increase in the signal $s(t)$ triggers a transition from the uncommitted steady state $\mathcal{O}$ to the committed steady states $\mathcal{A}$ or $\mathcal{B}$ in the vicinity of the pitchfork bifurcation singularity [Fig. 2(b)]. To obtain the respective probabilities of selecting $\mathcal{A}$ or $\mathcal{B}$ in these limits, we use an approach similar to Refs. [20,21] consisting of studying the Fokker–Planck equation associated with Eq. (1) where $F_P$ is linearized for small $x$ as $F_P(x,\alpha,s) \approx \alpha + \beta_1(s - 0.5)x$. The solution for the probability density function obtained by using the methods of characteristics is a Gaussian whose center $\mu(t,\alpha)$ and variance $V(t)$ evolve in time:

$$P(x,t,\alpha) = [2\pi V(t)]^{-1/2} e^{\frac{-[x-\mu(t,\alpha)]^2}{2V(t)}}, \tag{5}$$

where

$$\mu(t,\alpha) = \alpha e^{w(t)}\left(\frac{2}{\beta_1} + \int_0^t e^{-w(u)}du\right), \tag{6}$$

$$V(t) = \sigma^2 e^{2w(t)}\left(\frac{1}{\beta_1} + \int_0^t e^{-2w(u)}du\right), \tag{7}$$

with $w(t) = \beta_1 \int_0^t [s(u) - 0.5] du$. After crossing the pitchfork bifurcation point for $s > s_c$, the presence of an unstable fixed point near $x = 0$ splits the Gaussian distribution into two parts that rapidly spread out to $+\infty$ and $-\infty$, respectively [or steady states $x_\mathcal{A}$ and $x_\mathcal{B}$ when taking into account higher-order terms of the original scalar field given by Eq. (4)]. The probability $\mathcal{P}_\mathcal{A}$ of being in the attraction basin of $\mathcal{A}$ at time large enough but smaller than the Kramers' escape time from $\mathcal{A}$ can be approximated as

$$\mathcal{P}_\mathcal{A}(\alpha) = \lim_{t \to +\infty} \int_0^{+\infty} P(x,t,\alpha) dx. \tag{8}$$

### B. Asymptotic expressions for decision sensitivity

Computation of decision sensitivity $\eta$ in various asymptotic limits requires estimating the infinitesimal effect of $\alpha$ on the respective probabilities to select $\mathcal{A}$ or $\mathcal{B}$. By replacing Eq. (5) in Eq. (8), the probability change due to a positive increment of $\alpha$ reads $\delta \mathcal{P}_\mathcal{A} = \lim_{t \to \infty} \mathrm{erf}\left(\frac{\mu(t,\alpha)}{2V(t)}\right)/2$, which can be linearized for small $\alpha$ as $\delta \mathcal{P}_\mathcal{A} \approx \lim_{t \to \infty} \mu(t,\alpha)/\sqrt{2\pi V(t)}$. Replacing $\mu(t,\alpha)$ and $V(t)$ given respectively by Eqs. (6) and (7) and deriving with respect to $\alpha$ leads to

$$\eta = \frac{\left(\frac{2}{\beta_1} + \int_0^\infty e^{-w(u)} du\right)}{\sqrt{2\pi \sigma^2 \left(\frac{1}{\beta_1} + \int_0^\infty e^{-2w(u)} du\right)}}. \tag{9}$$

*Slow signal change.* In the large-$\tau$ limit, attractor selection is made during a finite time interval for which signal increases almost linearly as $s(t) \approx \frac{t - t_c}{2\tau} + 0.5$ for which $w(t) \approx \frac{\beta_1}{4\tau}(t - t_c)^2 - \frac{\beta_1 t_c^2}{4\tau}$. Substituting $w(t)$ into Eq. (9), integrating using rescaled time $\tilde{t} = t - t_c$, and keeping only the dominant term for large $\tau$ finally gives

$$\eta_{\tau \to \infty} = \left(\frac{2}{\pi \beta_1}\right)^{1/4} \tau^{1/4} \sigma^{-1}. \tag{10}$$

The formula is valid in the asymptotic limits of $\tau$ large and $\sigma$ small, provided that $\tau$ remains smaller than the Kramers' escape time $\tau_K \propto e^{\sigma^{-2}}$. This requirement reads $\sigma^2 \ln \tau \ll 1$.

*Fast signal change.* In the small-$\tau$ limit, the decision between $\mathcal{A}$ or $\mathcal{B}$ is made after the signal is quickly relaxed and saturated to 1 [i.e., $s(t) \approx 1$] for which $w(t) \approx \frac{\beta_1}{2} t$. Inserting $w(t)$ into Eq. (9) and integrating yields

$$\eta_{\tau \to 0} = \frac{2}{\sqrt{\pi \beta_1}} \sigma^{-1}. \tag{11}$$

Note that $\eta$ does not depend on the signal timescale $\tau$ anymore.

### C. Numerical simulations and crossover regimes

In the section above, distinct scaling behaviors for $\eta$ have been obtained in the limits of small noise and slow or fast signal changes. The range of validity of these expressions is assessed through numerical integration of the dynamical system (1) with the force field given by Eq. (4) (rather than integration of Fokker–Planck equation that is inefficient for very small noise). Numerical simulations agree with predicted scaling behaviors for $\eta$ given by Eqs. (10) and (11) for $\tau \ll \tau_c$ and $\gg \tau_c$, respectively, as long as $\sigma$ is below some critical noise $\sigma_c$ [see the crossover for both Figs. 2(c) and 2(d)]. For

some range of noise above $\sigma_c$, small $\alpha$-induced changes of the Kramers' transition rates between $\mathcal{A}$ and $\mathcal{B}$ lead to $\eta \propto \sigma^{-2}$ [Fig. 2(d)].

On the one hand, the critical signal timescale $\tau_c$ that separates the regimes of fast versus slow signal-driven decisions is related with the characteristic time for trajectories to escape the neighborhood of the unstable fixed saddle point before to quickly transit to steady states. This decision time can be expressed as a function of the local instability exponent of the saddle, but also of the noise as $\propto |\ln(\sigma)|$ or $\propto |\ln(\sigma)|^{1/2}$ depending on whether the potential evolves quickly or slowly [20], indicating that $\tau_c$ depends on $\sigma$ in a subtle manner.

On the other hand, the critical level of noise $\sigma_c$ corresponds to the noise beyond which back-and-forth transitions between neighborhoods of $\mathcal{O}$, $\mathcal{A}$ and $\mathcal{B}$ become frequent enough to modify the probability density distribution of Eq. (5) and to prevent stable fate choices at large time. In the limits of large and small $\tau$, respectively, those transitions tend to occur either close to or far from the pitchfork bifurcation for which different Eyring–Kramers laws apply [22], which reveals that $\sigma_c$ slightly decreases with $\tau$ but remains nevertheless bounded with, numerically, $1 < \sigma_c < 2$. It is to note that, although the parameter $\beta_2$ (i.e., whether the bifurcation is subcritical or supercritical) does not influence the asymptotic regimes consistently with linear approximations, it modifies the Kramers' escape rate so as to slightly change $\sigma_c$.

## IV. OSCILLATORY MECHANISM

### A. Transition from oscillation to bistability

We now investigate an alternative binary decision scheme based on the occurrence of limit-cycle bifurcations. Among the possible bifurcation scenarios, we consider the case where two stable fixed points appear through two saddle-node bifurcations on invariant circle (two-SNIC) [14]. In contrast with homoclinic bifurcations or saddle-node bifurcation of limit cycles, the two-SNIC bifurcation can be treated by using a one-dimensional model adapted from the theta model, acknowledged as the normal form of a SNIC bifurcation [23]. This two-SNIC theta model has a $2\pi$-periodic variable $x$ and is characterized by the scalar field

$$F_S(x,\alpha,s) = 1 - \cos(2x) - \alpha \cos(x) - \beta_3(s - 0.5)$$
$$\times [1 + \cos(2x) + \alpha \cos(x)], \tag{12}$$

where $\beta_3 > 0$. The phase diagram as a function of $\alpha$ and $s$ [Fig. 3(a)] shows the existence of one oscillatory state $\mathcal{O}$ and two steady states $\mathcal{A}$ or $\mathcal{B}$ with a region of bistability $\mathcal{A}/\mathcal{B}$, but no region of multistability involving $\mathcal{O}$ in contrast with the subcritical pitchfork bifurcation scenario. For $\alpha = 0$, transition from the oscillatory regime to the bistable regime occurs for $s \equiv s_c = 0.5$ through two simultaneous saddle-node bifurcations located at $x_{sn_\mathcal{A}} = 0$ and $x_{sn_\mathcal{B}} = \pi$, whereas the sign of $\alpha$ determines which attractor appears first and which is more stable. A temporal increase in signal $s(t)$ thus triggers a transition from the oscillatory state to one of the two committed steady states depending on the system state when saddle-node bifurcations occur [Fig. 3(b)]. Like for the pitchfork model, attractor selection induced by slow or fast signal variations in the low-$\alpha$ and -$\sigma$ limits is analyzed by studying temporal evolution of probability density and current, $P(x,t,\alpha)$ and
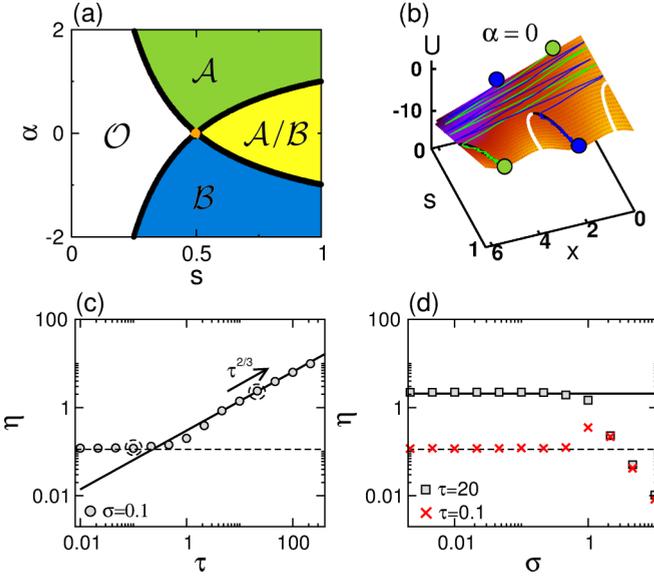
FIG. 3. (Color online) Binary decision making based on limit-cycle bifurcation [Eq. (12) with $\beta_3 = 2$]. (a) Phase diagram where $s$ is considered as a parameter. $\mathcal{O}$ is an oscillatory state whereas $\mathcal{A}$ and $\mathcal{B}$ are steady states. (b) Potential landscape and bifurcation diagram [black (white) lines: stable (unstable) steady-state branches] for $\alpha = 0$ with two examples of noisy trajectories. (c), (d) $\eta$ as a function of $\tau$ and $\sigma$ in numerical simulations (circles, squares, and crosses) as compared with the theoretical predictions of Eqs. (17) (solid lines) and (19) (dashed lines).

$J(x,t,\alpha)$, obeying the Fokker–Planck equation with periodic boundary conditions. The probability of being in the attraction basin of $\mathcal{A}$ (at time large enough but smaller than the Kramers' escape time from $\mathcal{A}$) is given by

$$\mathcal{P}_{\mathcal{A}}(\alpha) = \lim_{t \to +\infty} \int_{x_{s_1}(\alpha)}^{x_{s_2}(\alpha)} P(x,t,\alpha)dx, \quad (13)$$

where $x_{s_1}(\alpha)$ and $x_{s_2}(\alpha)$ are the two saddle points (i.e., attractor basin boundaries) for $s = 1$ satisfying $F_S(x_{s_{1,2}}, \alpha, s = 1) = 0$.

### B. Asymptotic expressions for decision sensitivity

Although an approximated solution for the probability distribution cannot be obtained, perturbative methods and symmetry assumptions are nevertheless sufficient to derive scaling laws for decision sensitivity $\eta$. Provided that the probability density distribution is stationary for $t \leqslant 0$, the probability density and current solutions of the corresponding Fokker–Planck equation can be expanded for $t \geqslant 0$ and small $\alpha$ as

$$P(x,t,\alpha) = P_0(x,t) + \alpha P_1(x,t), \quad (14a)$$

$$J(x,t,\alpha) = J_0(x,t) + \alpha J_1(x,t). \quad (14b)$$

Because the force field in Eq. (12) can be decomposed into two-fold rotational symmetric and skew-symmetric parts as $F_S(x,\alpha) = F_{S,0}(x) + \alpha F_{S,1}(x)$ where $F_{S,0}(x) = F_{S,0}(x + \pi)$ and $F_{S,1}(x) = -F_{S,1}(x + \pi)$, zero- and first-order solutions of probability density and current satisfy $P_0(x,t) = P_0(x + \pi,t)$ and $P_1(x,t) = -P_1(x + \pi,t)$ (respectively, $P \to J$).

*Slow signal change.* In the large-$\tau$ limit, small $\alpha > 0$ induces a differential slowing of trajectories near the respective saddle-node bifurcation occurrence, which progressively skews the distribution $P(x,t,\alpha)$ with a larger peak just before $x_{sn_{\mathcal{A}}}$ (as compared to before $x_{sn_{\mathcal{B}}}$), resulting in increasing $\mathcal{P}_{\mathcal{A}}$. Such an increase is captured by the time integration of the shift $\Delta J$ between inward and outward probability currents on a domain containing $x_{\mathcal{A}}$; for instance, $[x_{sn_{\mathcal{B}}}; x_{sn_{\mathcal{A}}}]$. Using Eq. (14b) and the associated symmetry properties, we obtain $\Delta J = 2\alpha J_1(x_{sn_{\mathcal{B}}}, t)$ so that binary choice sensitivity reads

$$\eta_{\tau \to \infty} = 2 \int_0^{+\infty} J_1(\pi, t)dt. \quad (15)$$

To derive the scaling behavior of $\eta$, we thus study the local dynamics near saddle-node bifurcation occurring at $x_{sn_{\mathcal{B}}}$ and $t_{sn} = \tau \ln 2$ where $F_S(x) \approx 2(x - \pi)^2 - \frac{\beta_3}{2\tau}(t - t_{sn}) + \alpha$. Under the following scaling transformations, $\tilde{\tau} = 2\tau/\beta_3$, $\tilde{t} = (\tilde{\tau}/2)^{-1/3}(t - t_{sn})$, $\tilde{x} = (4\tilde{\tau})^{1/3}(x - \pi)$, $\tilde{\alpha} = (\sqrt{2}\tilde{\tau})^{2/3}\alpha$ and $\tilde{\sigma} = (2\tilde{\tau})^{1/2}\sigma$, local dynamics close to saddle-node bifurcation satisfies a $\tau$-invariant Riccati nonlinear differential equation

$$\frac{d\tilde{x}}{d\tilde{t}} = \tilde{x}^2 - \tilde{t} + \tilde{\alpha} + \tilde{\sigma}\zeta(\tilde{t}). \quad (16)$$

We now define probability densities $p$ and $\tilde{p}$ and probability currents $j$ and $\tilde{j}$ which obey Fokker–Planck equations associated with Eqs. (15) and (16) supplemented with periodic boundary conditions at arbitrary $\pm x_c$: $p(x_c, t) = p(-x_c, t)$ and $\tilde{p}(\tilde{x}_c, \tilde{t}) = \tilde{p}(-\tilde{x}_c, \tilde{t})$. We also define the quantities

$$h(x,t) = \int_{t_{sn}-t_c}^{t_{sn}+t_c} \frac{dJ}{d\alpha}(x,t)dt,$$

$$\tilde{h}(\tilde{x}, \tilde{t}) = \int_{-\tilde{t}_c}^{\tilde{t}_c} \frac{d\tilde{J}}{d\tilde{\alpha}}(\tilde{x}, \tilde{t})d\tilde{t}.$$

The normalization $\int p(x,t)dx = \int \tilde{p}(\tilde{x}, \tilde{t})d\tilde{x} = 1$ results in the scaling relations $p = (4\tilde{\tau})^{1/3}\tilde{p}$, $j = (\tilde{\tau}/2)^{-1/3}\tilde{j}$, and $h = (\sqrt{2}\tilde{\tau})^{2/3}\tilde{h}$. Zero-order expansion of the functions $\tilde{p}$, $\tilde{j}$, and $\tilde{h}$ in the limit of small $\tilde{\sigma}$ allows us to rewrite $h = (\sqrt{2}\tilde{\tau})^{2/3}[h_0 + O(\tau\sigma^2)]$. Because $\eta$ in the original two-SNIC dynamical system follows the same scaling behavior as $h$ in the Riccati dynamical system, we write to leading order

$$\eta_{\tau \to \infty} = C\left(\frac{\tau}{\beta_3}\right)^{2/3}, \quad (17)$$

where $C \approx C_0 + O(\tau\sigma^2)$ (where numerical integration of the Langevin equation gives $C_0 \approx 0.492$), which indicates that $\eta$ is insensitive to noise as long as $\tau\sigma^2$ is small enough.

*Fast signal change.* In the small-$\tau$ limit, the probability of selecting attractor $\mathcal{A}$ (respectively, $\mathcal{B}$) given by Eq. (13) depends only on the initial probability distribution $P(x,0,\alpha)$ and the attractor boundaries given by the saddle point coordinates $x_{s_{1,2}}$ for $s = 1$:

$$\mathcal{P}_{\mathcal{A}}(\alpha) = \int_{x_{s_1}(\alpha)}^{x_{s_2}(\alpha)} P(x,0,\alpha)dx. \quad (18)$$

To compute $\eta$, we first expand Eq. (18) to first order in $\alpha$ using Eq. (14a) and $x_{s_i}(\alpha) = x_{s_i}(0) + (-1)^i \alpha \delta x_s$ (for $i = 1, 2$) and

we then derive with respect to $\alpha$ to obtain

$$\eta_{\tau \to 0} = \sum_{j=1,2} P_0(x_{s_j}(0),0)\delta x_{s_j} + \int_{x_{s_1}(0)}^{x_{s_2}(0)} P_1(x,0)dx, \quad (19)$$

where, after expanding $F_S(x_{s_{1,2}},\alpha,s=1)=0$, $\delta x_s$ reads

$$\delta x_{s_j} = \frac{1}{4|\sin[x_{s_j}(0)]|}. \quad (20)$$

In the particular case of $\beta_3 = 2$, we have $x_{s_2} = \pi/4$, $P_0(x,0) = (2\pi)^{-1}$ and $P_1(x,0) = 0$, whose substitutions into Eqs. (20) and (19) yield $\eta_{\tau \to 0} \approx 2^{-3/2}\pi^{-1}$. In the more general case of $\beta_3 \neq 2$, $\sigma$ might nevertheless influence $\eta$ by shaping $P(x,0)$.

### C. Numerical simulations and crossover regimes

Like for the pitchfork model, numerical simulations agree with predicted scaling behaviors for $\eta$ in Eqs. (17) and (19) for $\tau \gg \tau_c$ or $\ll \tau_c$ respectively, as long as $\sigma$ is below some critical value [see the crossover for both Figs. 3(c) and 3(d)]. Kramers' theory can again be used to estimate the critical noise $\sigma_c$ beyond which transitions between $\mathcal{A}$ and $\mathcal{B}$ above the two saddle points for $s = 1$ becomes frequent enough to influence choice probability and to explain the scaling behavior $\eta \propto \sigma^{-2}$ observed above $\sigma_c$, which is similar to the pitchfork model. However, in contrast with the pitchfork mechanism, the critical signal timescale $\tau_c$ that separates the slow versus fast signal-driven decision regimes is now related with the oscillation period (equal to $T_{\text{osc}} = \pi/\sqrt{2\beta_3}$ for $s = 0$ and $\alpha = 0$) and is thus not dependent on noise.

## V. GENERALIZED MODEL

For simplicity, the binary decision model introduced in Sec. II assumes the existence of symmetry properties so that $\mathcal{P}_\mathcal{A}(\alpha) = \mathcal{P}_\mathcal{B}(-\alpha)$ as well as of additive noise. However, protein network regulating cell-fate decisions exhibits a high-dimensional dynamics without particular symmetry, in which stochasticity (due for instance to finite number of proteins) is often modeled as multiplicative noise. In this section, we check whether our results are still valid with less restrictive assumptions by discussing the following generalized model:

$$\frac{dx}{dt} = g(x)F_{P,S}(x,\alpha,s(t,\tau)) + \sigma h(x)\zeta(t), \quad (21)$$

where $g(x)$ and $h(x)$ are arbitrary positive-valued function, whereas $g(x) = 1$ and $h(x) = 1$ in the original model. $h(x)$ leads to multiplicative noise, and $g(x)$ contributes to force-field asymmetry since $F_P(x,0,s)$ and $F_S(x,0,s)$ exhibit, respectively, reflection and two-fold rotational symmetry with respect to $x$. In fact, the asymptotic expressions previously obtained for $\eta$ in Eqs. (10), (11), (17), and (19) remain valid in such generalized model. For the pitchfork model in the low-noise limit, the decision outcome depends only on the local force and noise fields near the bifurcation point. Accordingly, Eqs. (10) and (11) apply for arbitrary $g$ or $h$ by replacing $\sigma$ with $\sigma h(0)/\sqrt{g(0)}$ and $\tau$ with $\tau/g(0)$. However, the validity range of these asymptotic expressions for increasing levels of noise strength is reduced due to larger deviations from Gaussian distribution. The case of the two-SNIC model is less straightforward as low-noise decision making depends
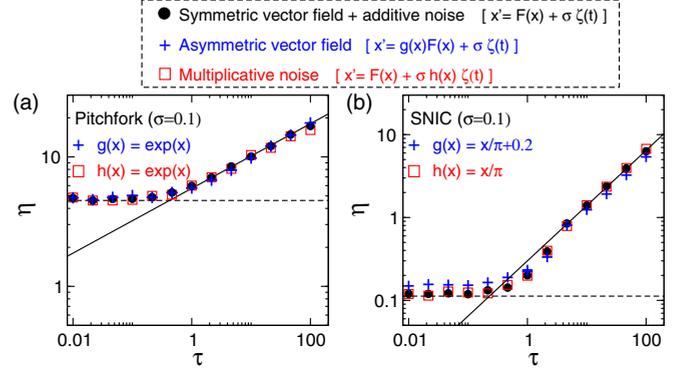


FIG. 4. (Color online) Effects of asymmetric force field and multiplicative noise. $\eta$ as function of $\tau$ for $\sigma = 0.1$ for (a) the pitchfork model and (b) the two-SNIC model with asymmetric force field (blue crosses) and multiplicative noise (red squares) as compared with original results (black circles) of Figs. 2(c) and 3(c).

(i) on the nonlocal initial probability distribution for small $\tau$ or (ii) on the dynamics close to two remote saddle-node bifurcation points for large $\tau$. As a consequence, a force field without two-fold rotational symmetry leads to different prefactors in Eqs. (17) and (19) for $\eta$, while keeping the same scaling relation with $\tau$ and $\sigma$. In contrast, multiplicative noise does not have any effect as far as $\eta$ does not depend on the noise component ($\tau\sigma^2$ small). Figure 4 illustrates that an asymmetric force field and multiplicative noise associated with some function $g(x)$ and $h(x)$ do not alter the scaling laws for $\eta$. We thus conjecture that the binary decision made by a protein network whose high-dimensional dynamics can be mapped onto a one-dimensional dynamics in the form of Eq. (21) follows the same scaling properties with respect to noise strength and signal timescale.

## VI. DISCUSSION

Binary decision is an important class of decision problems, especially for biological decision making. We have shown that binary decision implemented by a transition from oscillation to bistability is much more robust with respect to noise but more sensitive to signal timing as compared with decisions based on a transition from monostability to bistability. Compared to a mere stable fixed point, oscillations give rise to a much more dynamical ground state of decision, in which phase dynamics obliterates the diffusive effect of noise but also sensitizes decision outcomes to signal timing (with respect to the oscillator's phase) and signal risetime (with respect to the oscillator period). Noteworthily, decisional sensitivity to signal timing is not necessarily a problem because phase dynamics can be regulated individually and collectively; for instance, through the synchronization of coupled oscillators [24,25]. Binary decision based on oscillations is expected to be relevant to systems subject to uncontrollable and detrimental stochasticity, while being driven by dynamic and tunable signals, such as for fate decisions in cellular systems.

The pending question is what could be these intracellular oscillations contributing to cellular decision making. The cell-cycle oscillator is a natural candidate as various fate

decisions including quiescence, differentiation, stress response, or programed death usually coincides with cell-cycle arrest, which is dynamically implemented by few possible bifurcation mechanisms [26,27]. Distinct fate decisions have been shown to depend on the cell-cycle phase at which the signal is received and the cell-cycle progression is arrested, such as in Bacteria [28], Amoeba [29], C. Elegans [30] or mammals [31], which manifests the occurrence of binary differentiation decisions based on cell-cycle oscillations. There are also numerous signaling pathways capable of delivering both oscillatory and bistable responses, such as P53 or Notch-Hes1 signaling, many of which have been shown to contribute to binary fate responses upon stress or developmental signals [15–17]. Yet these different cell-cycle or signaling oscillatory mechanisms support the same notion of time windows for decision opportunities underlying complex signal processing.

More generally, the existence of distinct binary decision-making strategies in fluctuating environments is not restricted to individual cells based on the dynamics of their intracellular protein networks. Likewise, multicellular organisms have evolved neuronal networks implementing various bifurcation mechanisms, including limit cycle bifurcations, to also perform two-choice decision tasks [32,33]. In any case, the selection through learning or evolution of one or another decision-making strategy is likely to correlate with the adaptive tradeoffs specific to a particular biological context.

[1] C. H. Waddington, *The Strategy of the Genes: A Discussion of Some Aspects of Theoretical Biology* (George Allen & Unwin, London, 1957).

[2] D. Jukam and C. Desplan, Curr. Opin. Neurobiol. **20**, 6 (2010).

[3] H. H. Chang, M. Hemberg, M. Barahona, D. E. Ingber, and S. Huang, Nature (London) **453**, 544 (2008).

[4] N. R. Nene, J. Garcia-Ojalvo, and A. Zaikin, PLoS ONE **7**, 32779 (2012).

[5] N. R. Nene and A. Zaikin, Phys. Rev. E **87**, 012715 (2013).

[6] L. Billings, I. B. Schwartz, M. McCrary, A. N. Korotkov, and M. I. Dykman, Phys. Rev. Lett. **104**, 140601 (2010).

[7] C. Furusawa and K. Kaneko, Science **338**, 215 (2012).

[8] S. Huang, Y. P. Guo, G. May, and T. Enver, Dev. Biol. **305**, 695 (2007).

[9] R. Guantes and J. F. Poyatos, PLoS Comput. Biol. **4**, 1000235 (2008).

[10] J. Wang, L. Xu, E. Wang, and S. Huang, Biophys. J. **99**, 29 (2010).

[11] C. Furusawa and K. Kaneko, J. Theor. Biol. **209**, 395 (2001).

[12] A. Koseska, A. Zaikin, J. Kurths, and J. Garcia-Ojalvo, PLoS ONE **4**, 4872 (2009).

[13] N. Suzuki, C. Furusawa, and K. Kaneko, PLoS ONE **6**, 27232 (2011).

[14] B. Pfeuty and K. Kaneko, Phys. Biol. **6**, 046013 (2009).

[15] R. Kageyama, Y. Niwa, H. Shimojo, T. Kobayashi, and T. Ohtsuka, Curr. Top. Dev. Biol. **92**, 311 (2010).

[16] J. E. Purvis, K. W. Karhohs, C. Mock, E. Batchelor, A. Loewer, and G. Lahav, Science **336**, 1440 (2012).

[17] D. Schultz, M. Lu, T. Stavropoulos, J. Onuchic, and E. Ben-Jacob, Sci. Rep. **3**, 166 (2013).

[18] J. R. Busemever and J. T. Townsend, Psych. Rev. **100**, 432 (1993).

[19] P. L. Smith and R. Ratcliff, Trends Neurosci. **3**, 161 (2004).

[20] B. Caroli, C. Caroli, B. Roulet, and D. Saint-James, Phys. A **108**, 233 (1981).

[21] D. K. Kondepudi and G. W. Nelson, Nature (London) **314**, 438 (1985).

[22] N. Berglund and B. Gentz, Markov Processes Relat. Fields **16**, 549 (2010).

[23] B. Ermentrout and N. Kopell, SIAM J. Appl. Math. **46**, 233 (1986).

[24] R. Wang, K. Liu, L. Chen, and K. Aihara, Bioinformatics **27**, 3158 (2011).

[25] S. Ares, L. G. Morelli, D. J. Jorg, A. C. Oates, and F. Julicher, Phys. Rev. Lett. **108**, 204101 (2012).

[26] B. Pfeuty, Phys. Rev. E **86**, 021917 (2012).

[27] B. Pfeuty, PLoS ONE **7**, 35291 (2012).

[28] J. C. Meeks, E. L. Campbell, M. L. Summers, and F. C. Wong, Arch. Microbiol. **178**, 395 (2002).

[29] W. Jang and R. H. Gomer, Eukariot. Cell **10**, 150 (2011).

[30] V. Ambros, Development **126**, 1947 (1999).

[31] S. Pauklin and L. Vallier, Cell **155**, 135 (2013).

[32] L. Alabantakis and G. Deco, PLoS Comput. Biol. **7**, 1002086 (2011).

[33] P. Theodoni, G. Kova, M. W. Greenlee, and G. Deco, J. Neurosci. **31**, 234 (2011).